Compositional Mapping of the Mature Anterior Cruciate Ligament-to-Bone Insertion

Dovina Qu,[1] Siddarth D. Subramony,[1] Adele L. Boskey,[2] Nancy Pleshko,[3] Stephen B. Doty,[4] Helen H. Lu[1,5]

[1]Biomaterials and Interface Tissue Engineering Laboratory, Department of Biomedical Engineering, Columbia University, New York, New York 10027, [2]Musculoskeletal Integrity Program, Hospital for Special Surgery, New York, New York 10021, [3]Tissue Imaging and Spectroscopy Laboratory, Department of Bioengineering, Temple University, Philadelphia, Pennsylvania 19122, [4]Analytical Microscopy Laboratory, Hospital for Special Surgery, New York, New York 10021, [5]Department of Biomedical Engineering, Columbia University, 1210 Amsterdam Avenue, 351 Engineering Terrace, MC 8904, New York, New York 10027

Received 24 June 2016; accepted 27 January 2017
Published online in Wiley Online Library (wileyonlinelibrary.com). DOI 10.1002/jor.23539

ABSTRACT: The anterior cruciate ligament (ACL)-to-bone interface constitutes a complex, multi-tissue structure comprised of contiguous ligament, non-mineralized fibrocartilage, mineralized fibrocartilage, and bone regions. This composite structure enables load transfer between structurally and functionally dissimilar tissues and is critical for ligament homeostasis and joint stability. Presently, there is a lack of quantitative understanding of the matrix composition and organization across this junction, especially after the onset of skeletal maturity. The objective of this study is to characterize the adult bovine ACL-to-bone interface using Fourier transform infrared spectroscopic imaging (FTIRI), testing the hypothesis that regional changes in collagen, proteoglycan, and mineral distribution, as well as matrix organization, persist at the mature insertion. It was observed that while collagen content increases continuously across the adult interface, collagen alignment decreases between ligament and bone. Proteoglycans were primarily localized to the fibrocartilage region and an exponential increase in mineral content was observed between the non-mineralized and mineralized regions. These observations reveal significant changes in collagen distribution and alignment with maturity, and these trends underscore the role of physiologic loading in postnatal matrix remodeling. Findings from this study provide new insights into interface organization and serve as benchmark design criteria for interface regeneration and integrative soft tissue repair. © 2017 Orthopaedic Research Society. Published by Wiley Periodicals, Inc. J Orthop Res

Keywords: insertion; interface; aging; fibrocartilage; ligament

The integration of soft and hard tissues through compositionally and structurally organized junctions is essential for musculoskeletal function. This organization is especially important at the interfaces where the anterior cruciate ligament (ACL) inserts into bone. Here, the soft and hard tissues are connected via a fibrocartilaginous enthesis which can be subdivided into non-mineralized and mineralized regions[1,2]: The non-mineralized fibrocartilage is contiguous with the ligament and consists of rounded fibrochondrocytes embedded in a types I and II collagen-rich, proteoglycan-containing matrix.[3,4] Meanwhile, the adjacent mineralized zone is characterized by hypertrophic chondrocyte-like cells within a type X collagen-containing mineralized matrix.[5,6] Additionally, mineral content increases monotonically across the enthesis.[7–10] These spatial differences in matrix composition contribute to graduated changes in mechanical properties[7] which serve to minimize the formation of stress concentrations and mediate load transfer between ligament and bone.[1,2]

Connecting the femur and tibia, the ACL is the primary stabilizer of the knee.[11] However, the ACL is also the most frequently injured knee ligament and the inability to reestablish the native ligament-to-bone insertion following ACL reconstruction compromises long-term graft stability and joint function.[12,13] To develop strategies for regenerating this multi-tissue junction, it is critical to establish an in-depth understanding of the structure-function relationships at the interface.[14] While the ACL-to-bone insertion has been extensively described histologically,[1,2,4,6] quantitative understanding of regional variations in matrix composition remain limited. Such in-depth analyses are essential for elucidating the structure-function relationships across this complex multi-tissue interface. However, direct measurement of insertion properties is challenging due to tissue heterogeneity and overall length scale, which ranges from 100 μm to 1 mm depending on species and age.[1,6,15] Spectroscopic imaging methods, which use specific vibrational modes of molecular components to generate compositional maps, have been successfully adapted for quantitative characterization of complex tissue interfaces, including those found at the junction between ligament and bone,[10] tendon and bone,[8,9] as well as cartilage and bone.[16] In particular, Fourier transform infrared spectroscopic imaging (FTIRI), a high-resolution and high-throughput imaging technique, can be used to concurrently analyze multiple extracellular matrix components from a single sample. These analyses have been shown to correlate well with biochemical and histological analyses of collagen, proteoglycans, and mineral.[16–18] Furthermore, collagen orientation can be determined from the ratio of the amides I and II band areas.[19,20]

Previously, matrix content, distribution, and organization across the ACL-to-bone insertion were quantitatively

Grant sponsor: Presidential Early Career Award for Scientists and Engineers; Grant sponsor: NIH-NIAMS; Grant number: AR055280; Grant sponsor: NIH Core Center; Grant number: AR046121; Grant sponsor: NIH Ruth L. Kirschstein National Research Service Award T32; Grant number: AR059038; Grant sponsor: National Science Foundation Graduate Research Fellowship.
Correspondence to: Helen H. Lu (T: +212-854-4071; F: +212-854-8725; E-mail: hhlu@columbia.edu)

evaluated using FTIRI in a skeletally immature bovine model.[10] It was reported that in young animals, while collagen content decreased, the amount of proteoglycans remained relatively uniform, and mineral content increased exponentially across the interface. Given the histological changes at the enthesis,[6,21] as well as differences in ACL healing potential[22] and mechanical properties[23] that have been observed to develop with age, a quantitative understanding of the interface in a skeletally mature model is also important. Moreover, from a clinical standpoint, knowledge of age-related changes at the insertion is crucial, as ACL injures occur in patients young and old, with the incidence of injury in patients aged 40 and older reportedly increasing.[24] The objective of this study, therefore, is to map the matrix composition and organization of the skeletally mature ACL-to-bone insertion, including regional changes in collagen, proteoglycan, and mineral, using FTIRI. Additionally, this study evaluates site-dependent differences between the femoral and tibial insertions. The bovine model was selected for this study because it has been shown to approximate the human ACL well in terms of size and proportion.[25] Moreover, an extensive body of work characterizing the bovine ACL insertion has been established, enabling direct comparison of our results to published histologic,[6] FTIRI,[10] and mechanical[7,26] studies of the ACL. Based on previous work on age-related changes in connective tissues such as ligament,[6,27] tendon,[28,29] and fibrocartilage,[21,30] it is anticipated that the mature enthesis will exhibit a well-organized, collagen-rich, proteoglycan-poor matrix, with structural differences also expected between the femoral and tibial insertion sites.[6,31] These quantitative and systematic analyses of the interface matrix will augment current understanding of the maturation of this complex transition, as well as provide much needed benchmark parameters for integrative and functional ACL reconstruction based on either modification of semitendinosus grafts or the design of a tissue engineered ACL graft.

METHODS

Sample Isolation

Bovine tibiofemoral joints from skeletally mature animals[6] (female, aged 2–5 years; $n = 5$) were obtained from a local abattoir (Green Village Packing Company, Green Village, NJ). The surrounding muscle, subcutaneous fascia, collateral ligaments, patella, patellar tendon, adipose tissue, and menisci were removed from each joint. The cruciate ligaments were then transected, and the femoral and tibial ACL insertions were identified and excised. Each sample ($\sim 5 \times 5 \times 2$ cm) was visually confirmed to contain intact and contiguous ligament, fibrocartilage, and bone regions and was bisected sagittally using a band saw for corresponding decalcified and non-decalcified analyses.

Sample Preparation

Decalcified samples were prepared for analysis of collagen and proteoglycan content and distribution. Immediately following harvest, samples ($n = 5$ per insertion site) were fixed for 72 h in 80% ethanol supplemented with 1% cetylpyridinium chloride (Sigma–Aldrich, St. Louis, MO) to preserve proteoglycans.[32] Following fixation, samples were rinsed in distilled water and demineralized in tris-hydroxymethylaminomethane buffer (Sigma–Aldrich, pH 7.2) containing 10% ethylenediaminetetraacetic acid (Sigma–Aldrich) over the course of 8 weeks, with solution exchange occurring every 3 days. Next, samples were dehydrated using an increasing ethanol series, cleared with xylenes, and embedded in paraffin (Fisher Scientific, Pittsburgh, PA). For FTIRI analysis, samples were sectioned (7 μm; Reichert-Jung RM 2030 Microtome, Leica, Bannockburn, IL) and placed immediately onto barium fluoride (BaF_2) infrared-transmissive windows (25×2 mm; Spectral Systems, Hopewell Junction, NY). Sections were then deparaffinized in xylenes, rehydrated, and then dried overnight at 25°C. Adjacent sections (7 μm) for histological analysis were collected on glass slides (Fisher Scientific) and dried overnight at 56°C.

Corresponding non-decalcified samples were prepared for mineral analysis, wherein samples were fixed for 72 h in 90% ethanol, dehydrated using an ethanol series, and then embedded in polymethylmethacrylate (PMMA; Sigma–Aldrich). For FTIRI analysis, samples were sectioned (2 μm) using a sliding microtome (SM2500S, Leica) fitted with a tungsten carbide blade (Delaware Diamond Knives, Wilmington, DE) and placed immediately onto BaF_2 windows and then dried overnight at 25°C. Adjacent sections (7 μm) for histological analysis were collected on Haupt's adhesive-treated glass slides, dried overnight at 65°C, and subsequently cleared of PMMA using a 1:1 xylene/chloroform (v/v) solution.

FTIRI and Spectral Analyses

Sample analysis was performed using an FTIR spectrometer (Spectrum 100, PerkinElmer, Waltham, MA) coupled to a microscope imaging system (Spotlight 400, PerkinElmer) following previously published methods.[10,16] Spectra (~20,000 points of spectral data per sample) were acquired between 2,000 and 800 cm^{-1} with a spectral resolution of 8 cm^{-1} and a spatial resolution of 25 μm (15 scans per pixel). IR spectra were analyzed and spectroscopic maps were generated using ISYS chemical imaging software (3.1.1., Spectral Dimensions, Olney, MD) and MATLAB (8.4.0. R2014b, The MathWorks, Natick, MA). Prior to analysis, spectra were corrected by baseline subtraction. For non-decalcified sections, sample spectra were additionally corrected for background from the PMMA embedding medium. Spectra of pure PMMA were acquired, baseline corrected, normalized by the highest peak in the PMMA spectrum (1,728 cm^{-1}) and then subtracted from similarly baseline-corrected and normalized sample spectra to eliminate PMMA background. This method was implemented to compensate for varying degrees of PMMA penetration into the multiple tissue types present across the interface.

Signature peaks within the collagen and carbohydrate spectra have been shown to correlate linearly with collagen and proteoglycan content.[33] Relative collagen content ($n = 5$) was mapped by integrating the peak area under the amide I band (1,720–1,590 cm^{-1}).[33,34] Proteoglycan distribution ($n = 5$) was estimated by integrating under the carbohydrate band associated with C–O–C and C–OH vibrations (1,140–985 cm^{-1}) and normalizing to the amide I band area to account for variations in section thickness and overlap between the collagen and carbohydrate spectra.[17,35]

Furthermore, collagen alignment ($n = 5$) was determined by collecting spectra with a gold-wire polarizer grid (PerkinElmer) inserted in the path of the infrared light, with the polarizer aligned at 0° with respect to the ligament-to-bone interface. Because amides I and II (1,590–1,492 cm^{-1}) bond vibrations are orthogonal, the ratio of their band areas is an indicator of collagen fibril orientation when spectra are collected under polarized light.[20] Numerical indices for collagen orientation were obtained by calculating the amide I/amide II area ratio. Collagen fibril orientation was categorized as parallel or perpendicular to the fibrocartilage-bone interface for any ratio greater than 2.7 or less than 1.7, respectively, while a ratio between 1.7 and 2.7 indicated mixed fibril orientation.[20] The relative mineral-to-matrix ratio ($n = 5$) in non-decalcified samples was calculated by integrating under the $\nu1$, $\nu3$ phosphate band contour (1,200–900 cm^{-1}) and dividing by the amide I band area. Mineral crystallinity was determined from the 1,030 cm^{-1}:1,020 cm^{-1} peak height ratio. As the 1,030 cm^{-1} peak is indicative of phosphate in stoichiometric apatites, while the 1,020 cm^{-1} peak represents nonstoichiometric apatites, the 1,030:1,020 intensity ratio provides a measure of mineral crystallinity and maturity, with higher ratios being associated with more crystalline mineral.[17,36] The 1,030:1,020 peak ratio was only calculated for mineralized tissue regions, as determined from the mineral distribution map.

Histology

To verify the compositional maps obtained using FTIRI, histology was also performed. Collagen distribution ($n = 5$) in decalcified samples was visualized by Picrosirius red staining (Sigma–Aldrich, 0.1% solution) and collagen orientation ($n = 5$) was imaged using a light microscope fitted with a polarized light filter (Olympus BX60, Olympus, Center Valley, PA). Proteoglycan ($n = 5$) distribution in decalcified samples was visualized by Safranin-O staining (Sigma–Aldrich, 0.6% solution), with collagenous tissues counterstained with fast green (Acros Organics, Geel, Belgium; 0.2% solution). Mineral distribution ($n = 5$) in non-decalcified samples was visualized by von Kossa staining, in which samples were incubated in a 5% silver nitrate solution (Fisher Scientific) in the presence of ultraviolet light, while soft tissues were counterstained with neutral red (Acros Organics).

Quantitative Analysis of Matrix and Mineral Distribution

Line profiles of relative collagen, proteoglycan, and mineral content ($n = 5$/outcome) extending across the insertion were generated from the spectral data. Tissue regions were identified based on corresponding histology and values for 100 equally spaced points spanning from ligament to bone were interpolated using a MATLAB bicubic least squares method. This normalization method allowed matrix content to be presented as a function of percent distance across the insertion, thereby accounting for any differences in fibrocartilage thickness among specimens. Line profiles were obtained across the width of each sample on a pixel-by-pixel basis and were then averaged, resulting in a single line profile representing the mean data collected for the sample. Regions exhibiting anomalies such as holes or folds were excluded. Average relative matrix and mineral content values were also calculated for each tissue region (ligament, non-mineralized fibrocartilage, mineralized fibrocartilage, and bone) and compared.

Statistical Analysis

The least significant number to establish significance ($p < 0.05$) between groups was determined to be $n = 5$ by power analysis of published FTIRI data on the immature bovine ACL insertion.[10] For this sample size, the statistical power of the region-wise comparison of mineral distribution and mineral crystallinity were 96% and 99%, respectively. Results are presented as mean ± standard deviation. Two-way analysis of variance (ANOVA) was performed to determine region- and insertion site-dependent differences in matrix or mineral content. The Tukey–Kramer post-hoc test was used for all pair-wise comparisons ($p < 0.05$). All statistical analyses were performed using JMP IN (4.0.4, SAS Institute, Cary, NC). Additionally, matrix content profiles across the interface were modeled using both linear ($y = Ax + B$) and exponential ($y = Ce^{D} + E$) functions to determine whether the observed spatial changes in matrix content are better modeled as continuous gradient or stepwise functions, respectively.

RESULTS

Spectra Analyses and Sample Size

The ligament, fibrocartilage, and bone regions each yielded characteristic spectra (Fig. 1). While both the amides I and II peaks were evident in all three tissue regions, the carbohydrate band indicative of proteoglycans was most prominent in the fibrocartilage areas, and the phosphate $\nu1$, $\nu3$ band was observed only in the mineralized fibrocartilage and bone regions. For each sample, the scan area was selected such that the ligament, fibrocartilage, and bone regions each occupied approximately one third of the total analysis area (Fig. 2). On average, the fibrocartilage interface spanned 396 ± 86 μm, with the non-mineralized zone

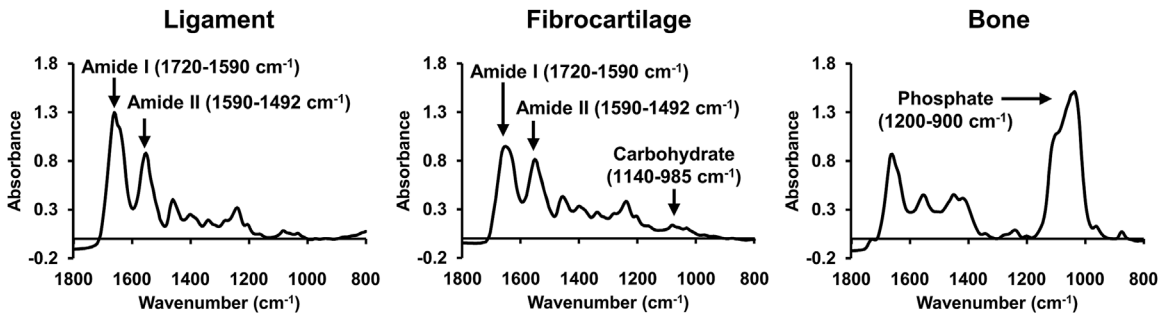

Figure 1. Representative infrared spectra of the ligament, fibrocartilage, and bone regions.

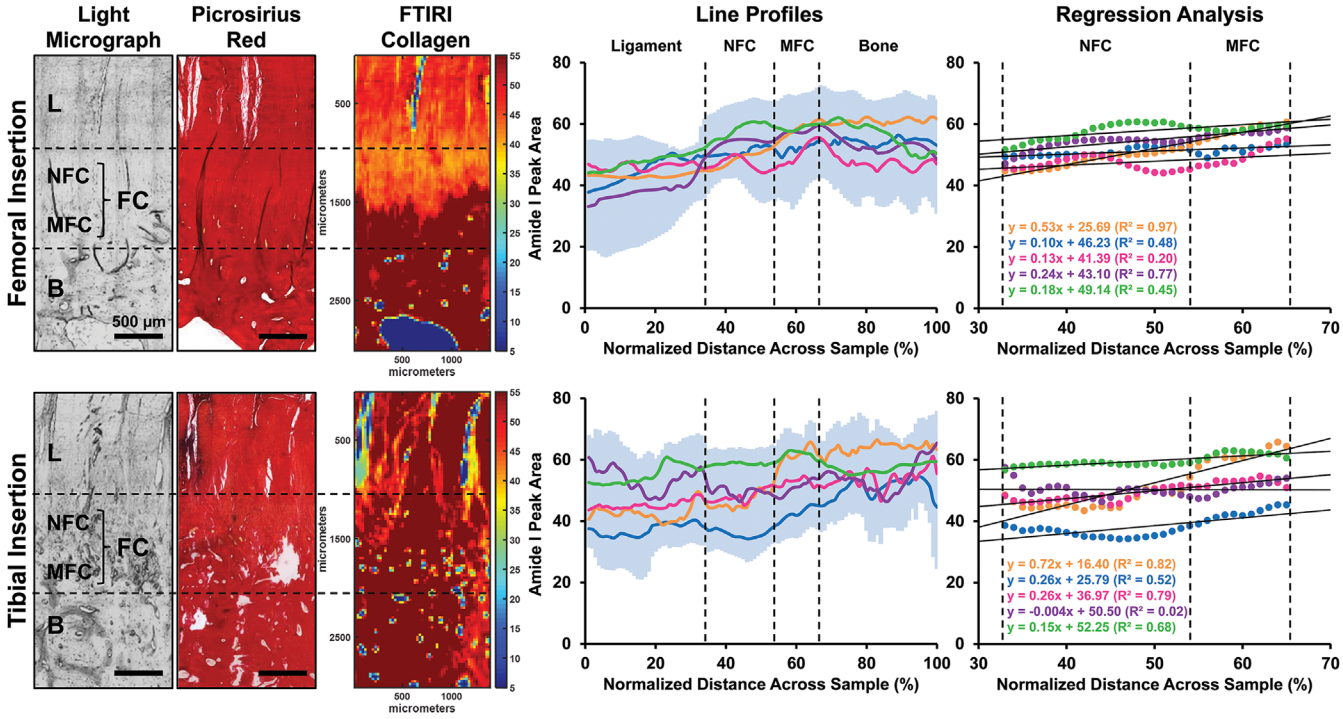

Figure 2. Collagen distribution. Light micrograph denotes the tissue regions across the ACL-to-bone insertion (L, ligament; NFC, non-mineralized fibrocartilage; MFC, mineralized fibrocartilage; B, bone). Picrosirius red staining confirms collagen presence across the insertion while FTIR spectroscopic maps (blue and red indicate low and high matrix content, respectively) and corresponding line profile analyses ($n = 5$, each solid line represents mean peak ratios and shaded area shows standard deviation for each sample) reveal a continuous increase in collagen content from ligament to bone, with the highest collagen content found in the bone region. Regression analysis of line profiles finds linear gradients in collagen content across the non-mineralized and mineralized fibrocartilage regions. No differences are observed between femoral and tibial insertions.

accounting for approximately 60% of the total fibrocartilage region.

Collagen Distribution and Organization

Quantita,tive mapping and histology of mature femoral and tibial insertions showed continuous collagen matrix spanning across the ligament, fibrocartilage, and bone regions (Fig. 2). Line profile analyses revealed that collagen content increased across the interface from ligament to bone. Linear regression analysis yielded positive slopes of 0.24 ± 0.17 for the femoral insertion and 0.28 ± 0.27 for the tibial insertion (Fig. 2), indicative of spatial increases in collagen content across the insertion. Comparison of the goodness of fit for exponential and linear models revealed that this distribution can be similarly modeled by exponential ($R^2 = 0.57 \pm 0.30$ for femoral samples, $R^2 = 0.56 \pm 0.34$ for tibial samples) and linear ($R^2 = 0.57 \pm 0.30$ for femoral samples, $R^2 = 0.56 \pm 0.34$ for tibial samples) functions (Table 1).

Collagen organization was assessed by both polarized FTIRI and polarized light microscopy of stained

Table 1. Modeling Matrix Distribution Across the Fibrocartilage

	Collagen	Proteoglycans	Mineral	Mineral Crystallinity
R^2_{Femoral}				
Exponential	0.57	0.40	0.97*	0.71
Linear	0.57	0.40	0.92	0.92*
p	**0.99**	**0.98**	**0.01**	**0.002**
R^2_{Tibial}				
Exponential	0.56	0.38	0.95*	0.61
Linear	0.56	0.38	0.93	0.85*
p	**0.99**	**0.99**	**0.03**	**0.02**

Comparison of the mean goodness of fit for exponential versus linear model indicated that the region-dependent difference in mineral content is best modeled by an exponential function (*$p < 0.05$), whereas collagen and proteoglycan distribution can also be well-modeled by linear functions ($p \gg 0.05$). The bolded values are the p-values for comparison of the linear versus exponential fits. The bolded formatting is intended to differentiate the p-values from the R-squared values.

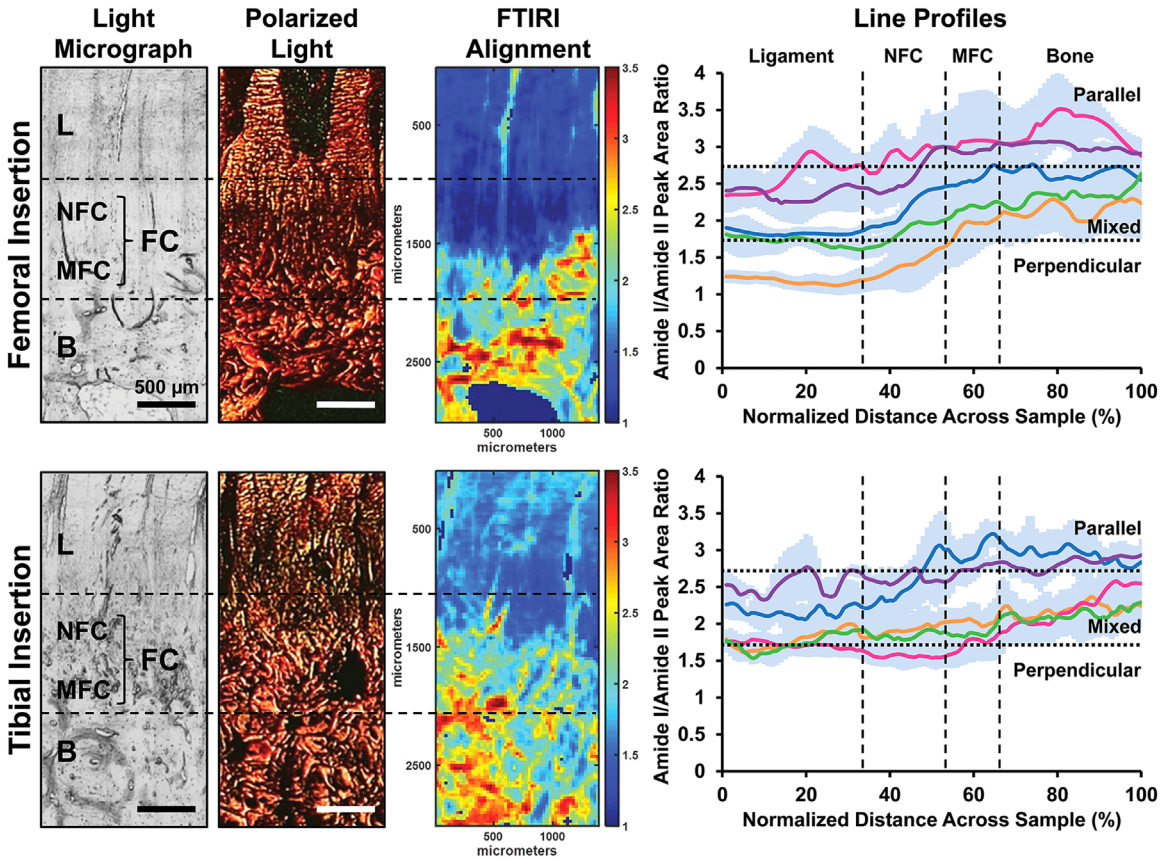

Figure 3. Collagen Organization. Light micrograph denotes the tissue regions across the ACL-to-bone insertion (L, ligament; NFC, non-mineralized fibrocartilage; MFC, mineralized fibrocartilage; B, bone). Polarized light images of Picrosirius red-stained sections corresponds to FTIR spectroscopic maps (blue perpendicular to ligament-bone interface; yellow, mixed orientation; red, parallel to ligament-bone interface. Corresponding line profile analyses ($n = 5$, each solid line represents mean peak ratios and shaded area shows standard deviation for each sample) reveal that collagen fibrils in the ligament region are predominantly oriented perpendicularly to the bone, while fibrils in the fibrocartilage regions are less organized and insert obliquely into the bone region. No differences are observed between femoral and tibial insertions.

sections (Fig. 3). Collagen fibrils in the ligament region were observed to be oriented perpendicularly relative to the ligament-to-bone interface. However, the fibrils change alignment across the fibrocartilage region, eventually inserting obliquely into the bone region. Overall, no significant differences in collagen distribution or alignment were observed between the femoral and tibial insertions.

Proteoglycan Distribution

FTIRI mapping and histology of mature femoral and tibial insertions confirmed that proteoglycans are primarily localized to the ligament and fibrocartilage regions (Fig. 4). Line profile analyses revealed that the highest relative proteoglycan content was found within the fibrocartilage zone. Linear regression analysis of the fibrocartilage region yielded an average slope of $(-2.28 \pm 1.81) \times 10^{-4}$ for the femoral insertion and $(-0.08 \pm 2.74) \times 10^{-4}$ for the tibial insertion (Fig. 4), indicating little change in proteoglycan content across this region. Comparison of the goodness of fit for exponential and linear models revealed that this distribution can be similarly modeled by exponential ($R^2 = 0.40 \pm 0.32$ for femoral samples, $R^2 = 0.38 \pm 0.39$ for tibial samples) and linear ($R^2 = 0.40 \pm 0.33$ for femoral samples, $R^2 = 0.38 \pm 0.39$ for tibial samples) functions (Table 1). Overall, no significant differences in proteoglycan distribution were observed between the femoral and tibial insertions.

Mineral Distribution and Maturity

Mineral was observed to be localized to the calcified fibrocartilage and bone regions, as evidenced from peak integration maps of the phosphate band normalized to the amide I band, as well as from histological staining (Fig. 5). Region-wise comparison revealed significantly higher mean mineral content in these regions compared to the ligament and non-mineralized fibrocartilage regions ($p < 0.05$, Fig. 6). Line profiles across the interface similarly showed an abrupt increase in mineral content between the non-mineralized and mineralized fibrocartilage regions. Regression analysis of the interface revealed that mineral distribution can be modeled by either an exponential ($R^2 = 0.97 \pm 0.02$ for femoral samples, $R^2 = 0.95 \pm 0.02$ for tibial

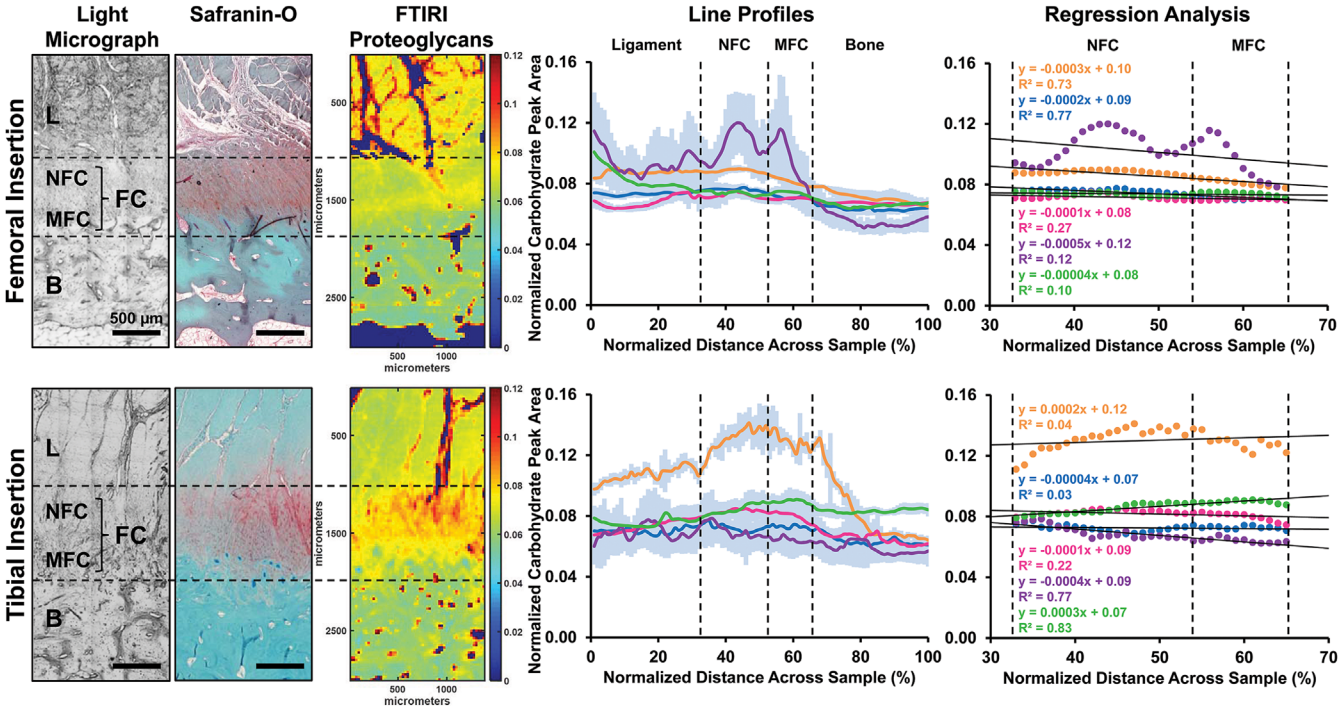

Figure 4. Proteoglycan distribution. Light micrograph denotes the tissue regions across the ACL-to-bone insertion (L, ligament; NFC, non-mineralized fibrocartilage; MFC, mineralized fibrocartilage; B, bone). Safranin-O with fast green counterstaining confirms proteoglycan presence at the insertion while FTIR spectroscopic maps (blue and red indicate low and high matrix content, respectively) and corresponding line profile analyses ($n = 5$, each solid line represents mean peak ratios and shaded area shows standard deviation for each sample) reveal the highest proteoglycan content is found in the fibrocartilage region. Regression analysis of line profiles finds little change in proteoglycan content across the non-mineralized and mineralized fibrocartilage regions. No differences are observed between femoral and tibial insertions.

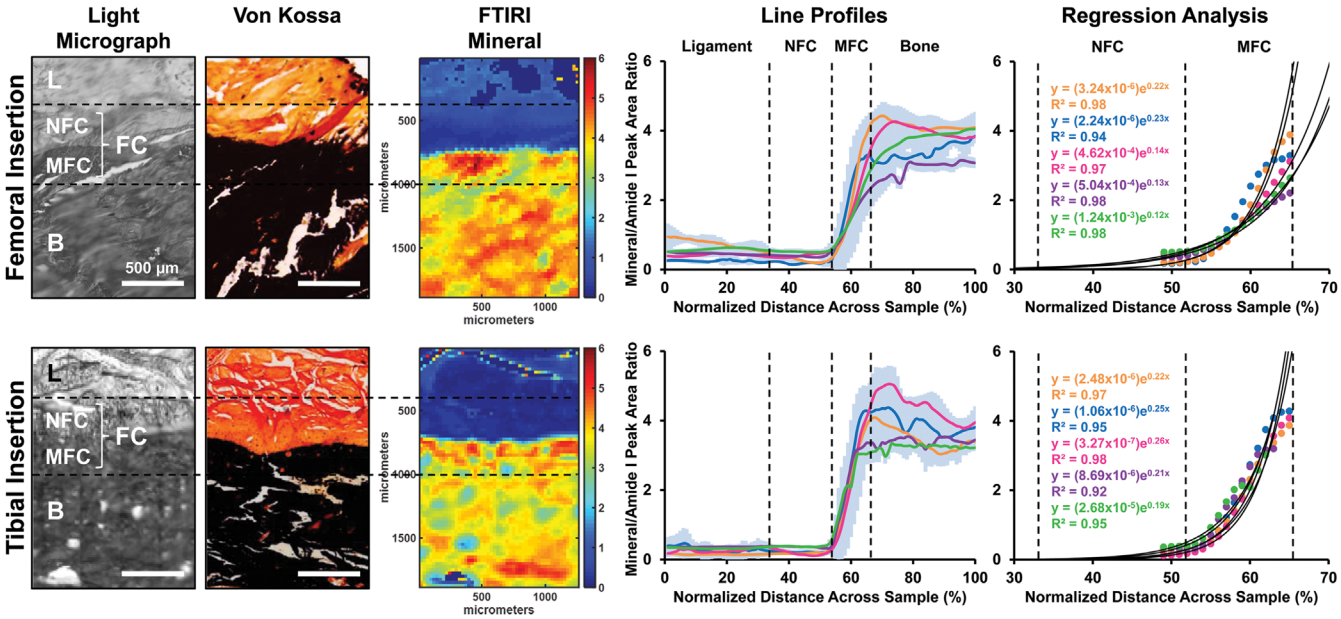

Figure 5. Mineral distribution. Light micrograph denotes the tissue regions across the ACL-to-bone insertion (L, ligament; NFC, non-mineralized fibrocartilage; MFC, mineralized fibrocartilage; B, bone). Von Kossa staining confirms mineral presence in the MFC and bone regions while FTIR spectroscopic maps (blue and red indicate low and high matrix content, respectively) and corresponding line profile analyses ($n = 5$, each solid line represents mean peak ratios and shaded area shows standard deviation for each sample) reveal an increase in mineral content from MFC to bone. Regression analysis of line profiles finds an exponential increase in mineral content across the mineralized fibrocartilage region. No differences are observed between femoral and tibial insertions.

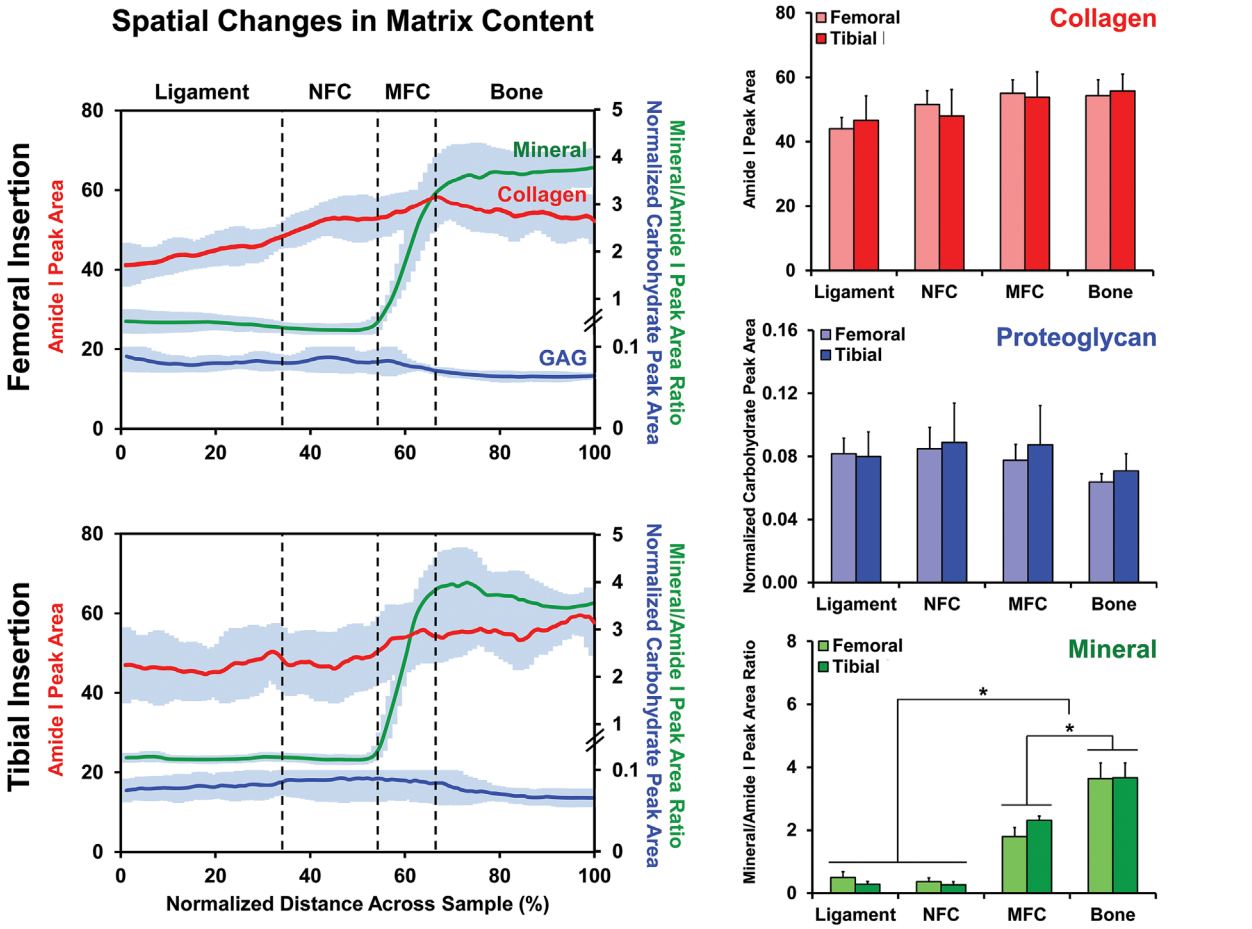

Figure 6. Regional comparison of matrix distribution. Average collagen content (red, $n = 5$) increases monotonically across the ACL-to-bone transition, though region-wise comparison shows no significant differences among tissue regions. Proteoglycan content (blue, $n = 5$) is the highest in the fibrocartilage zones, but region-wise comparison also showed no significant differences among tissue regions. Mineral content (green, $n = 5$) increases significantly between the non-mineralized (NFC) and mineralized (MFC) fibrocartilage zones, with the highest mineral content measured in the bone region. ($n = 5$, $^{*}p < 0.05$: differences between regions). No differences are found between femoral and tibial insertions.

samples) or a linear ($R^2 = 0.92 \pm 0.03$ for femoral samples, $R^2 = 0.93 \pm 0.01$ for tibial samples) function, though the exponential function yields a significantly higher goodness of fit for both insertion sites ($p < 0.05$, Table 1).

Mineral crystallinity was determined by evaluation of the 1,030:1,020 peak height ratio across the calcified tissue regions (Fig. 7). Region-wise comparison revealed a significantly higher mean 1,030:1,020 intensity ratio in the bone region (1.09 ± 0.05 for femoral samples, 1.07 ± 0.07 for tibial samples) compared to the mineralized fibrocartilage region (0.58 ± 0.07 for femoral samples, 0.65 ± 0.07 for tibial samples, $p < 0.05$). Regression analysis of the mineralized interface revealed a linear increase in crystallinity with an average slope of 0.10 ± 0.004 for the femoral insertion ($R^2 = 0.92 \pm 0.03$) and 0.09 ± 0.01 ($R^2 = 0.85 \pm 0.14$) for the tibial insertion (Table 1). Overall, no significant differences in mineral distribution or crystallinity were observed between the femoral and tibial insertions.

DISCUSSION

The interface between the ACL and bone consist of a fibrocartilaginous transition which has been shown to play a critical mechanical role in securing the ligament to bone. The objective of this study was to map matrix content, distribution, and organization across the ACL-to-bone insertion in a skeletally mature, large animal model, and to evaluate anatomical site-related compositional and structural differences across this complex junction. It was found that the mature enthesis exhibits a well-organized, collagen-rich, proteoglycan-poor matrix. Moreover, comparison to previous studies of the immature ACL-to-bone insertion[10] reveals substantial changes in interface matrix composition and organization, reflecting postnatal adaptations to the complex forces generated at the ligament-to-bone interface.

In this study, it was observed that the mature ACL insertion displayed a dense collagenous matrix spanning across all three regions of the interface with a trend of increasing collagen content progressing from

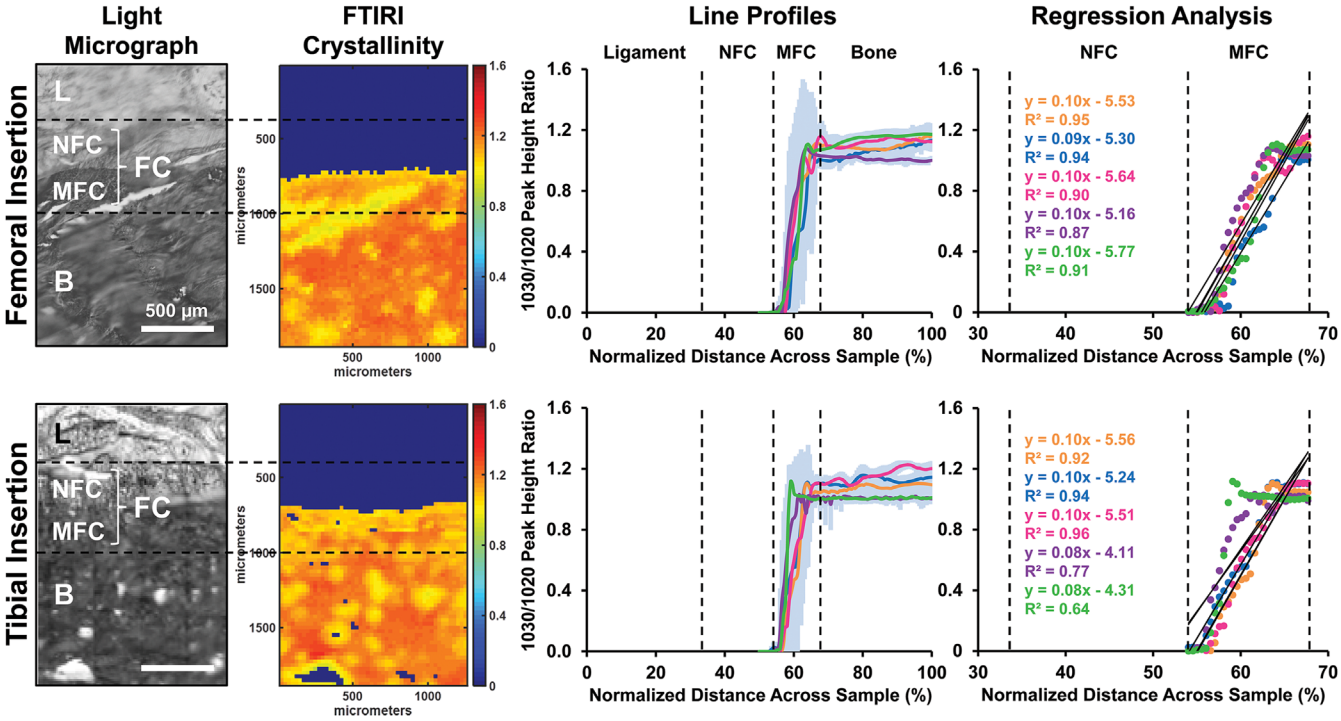

Figure 7. Mineral Crystallinity. Light micrograph denotes the tissue regions across the ACL-to-bone insertion (L, ligament; NFC, non-mineralized fibrocartilage; MFC, mineralized fibrocartilage; B, bone). FTIR spectroscopic maps (blue and red colors indicate low and high crystallinity, respectively) and corresponding line profile analyses (n = 5, each solid line represents mean peak ratios and shaded area shows standard deviation for each sample) reveal an increase in mineral crystallinity from MFC to bone. Regression analysis of line profiles finds a linear increase in mineral crystallinity across the MFC region. No differences are observed between femoral and tibial insertions.

ligament to bone. Polarized FTIRI analysis of collagen organization showed that while collagen fibrils in the ligament region were relatively perpendicular to the interface, the orientation of fibrils changes across the fibrocartilage and insert obliquely into bone. These results are consistent with published histological analysis of the adult enthesis, in which collagen fibrils were found to bridge the entire junction between ligament and bone, albeit with varying fibril size and arrangement observed between different zones.[1] A similar gradient in collagen organization between the non-mineralized and mineralized regions has also been reported for the rat supraspinatus tendon-to-bone interface.[37] Theoretical models have shown that this organizational gradient aids stress dissipation at the soft tissue to bone junction and helps to reduce requisite interface thickness.[37,38]

In addition to differences in the collagenous matrix, spatial changes in proteoglycan content were also observed. Proteoglycans are produced in response to compressive loads, consistent with previous studies of the ligament-to-bone insertion,[6,10,39] were found here to be predominantly localized to the fibrocartilage regions. Although the ligament is loaded primarily in tension, the entheses are subject to complex dynamic stress profiles which include tensile, shear,

Table 2. Comparison of Immature and Mature ACL-to-Bone Insertions

	Immature[10]	Mature
Collagen distribution	Highest in ligament, decreases across the insertion from ligament to bone	Highest in bone, increases across the insertion from ligament to bone
Collagen alignment	Fibers in ligament and fibrocartilage regions are parallel to the bone	Fibers in ligament region are perpendicular to bone, and mixed fiber orientation is observed across the insertion
GAG distribution	Relatively constant across the insertion	Relatively constant across the insertion
Mineral distribution	Exponential increase ($R^2 = 0.97$ for femoral, $R^2 = 0.95$ for tibial) in mineral content across mineralized fibrocartilage region	Exponential increase ($R^2 = 0.97$ for femoral, $R^2 = 0.99$ for tibial) in mineral content across mineralized fibrocartilage region

Collagen distribution and alignment across the insertion change with age. However, relative proteoglycan and mineral distributions are conserved over time.

and compressive components.[26,40] Additionally, the junction between the non-mineralized and mineralized tissue regions was marked by a sharp increase in mineral content, which is well modeled as an exponential gradient. Similar monotonic mineral gradients have also been observed at the tendon-to-bone enthesis,[8,9] where they serve to mediate load transfer and reduce the formation of stress concentrations. This zonal difference in mineral content has been correlated with an almost twofold increase in compressive modulus between non-mineralized and mineralized regions.[7]

Comparison to published FTIRI analysis[10] of the skeletally immature bovine insertion reveals marked age-related differences in matrix content and organization (Table 2). For the immature ACL-to-bone interface, collagen content was highest in the ligament and decreased across the enthesis.[10] Interestingly, the relative collagen content across the mature insertion is observed to be approximately twice that of the immature insertion, suggesting an overall increase in matrix density with age. These findings are consistent with published reports of age-related increases in collagen density in ligaments[27] and tendons[28] and correspondingly stiffer and more resilient tissue in older animals.[41] Moreover, in contrast to the substantial decrease in collagen content between the ligament and bone regions in immature samples,[10] collagen distribution across the mature interface is relatively consistent, reflecting compositional changes in the collagenous matrix with age. It has been reported that while the interzone between ligament and bone in young animals lacks type I collagen and resembles hyaline cartilage, type I collagen is found throughout all regions of the mature ligament-to-bone insertion.[6,41,42] Additionally, the mature fibrocartilage region is rich in types II and XIV collagen, which help to modulate tissue mechanical properties by mediating interactions between collagen fibers.[42] These changes in collagen composition may account for the differences in overall collagen content observed. Organization of collagen fibrils across the ACL-to-bone insertion also changes with age. Whereas collagen fibrils in the immature insertion are primarily oriented parallel to the interface,[10] ligament collagen fibrils were observed to insert perpendicularly into the mature insertion. These differences are consistent with polarized light microscopy observations.[6]

Proteoglycan content across immature interface was observed to be highest in the fibrocartilage regions and relatively uniform across these zones.[10] A similar distribution was found in the mature interface, though the low relative proteoglycan values suggest that proteoglycan content is reduced in the mature enthesis compared to in immature tissues. Histological studies of the ACL insertions[6] and other fibrocartilaginous tissues[21] have similarly reported decreasing proteoglycan content over time. These changes in content and organization are likely driven by repetitive tensile physiologic loading of the ligament.

In contrast to the changes in collagen and proteoglycan matrix, the relative mineral content and distribution were similar between mature and immature insertion sites, with mineral localized to the calcified fibrocartilage and bone regions and the relative mineral content increasing exponentially across the insertion.[10] However, differences in mineral crystallinity between the mineralized fibrocartilage and bone regions were observed in the mature insertion, which suggests that the mineralized matrix also continues to undergo postnatal remodeling. Analysis of postnatal changes in the mouse supraspinatus tendon-to-bone insertion showed that carbonate content of apatite mineral at the enthesis increases over time.[9] Moreover, age-related changes in alkaline phosphatase activity at the ACL enthesis and the appearance of higher mineral density in mature specimens have also been reported.[6] The similarity between the relative mineral content of the mature and immature insertions is reflective of the concurrent increase in collagen matrix in older animals which causes the mineral-to-matrix ratio to remain unchanged despite the increase in mineral content. It has been postulated that the mineral differential between the non-mineralized and mineralized regions serves different functions over the course of development, where it may play a mechanotransductive role early on, and then serves increasingly to stabilize the interface as the matrix matures and cellularity decreases.[9]

The spatial differences in composition and organization observed across the insertion reflect adaptions to the complex forces generated at the ligament-to-bone junction, with progressive changes in mechanical properties across the enthesis.[7] This structured organization minimizes the formation of stress concentrations and facilitates the attachment of mechanically dissimilar tissues. As the elastic modulus of bone is more than an order of magnitude greater than that of the ligament, the gradual transition in mechanical properties across the intermediary fibrocartilage regions helps to protect the soft tissue from contact deformation and damage.[43] Moreover, comparison of the composite organization of mature and immature entheses suggests that the matrix composition and structure of the ACL-to-bone insertion continue to change postnatally in response to these mechanical cues. It is well established that physiologic loading plays a critical role in enthesis development,[44] and studies of rat cruciate ligament enthesis development reported that these changes can yield a multifold increase in tissue stiffness.[41]

While no statistically significant differences in matrix distribution or organization were observed between the femoral and tibial insertions, which are known to differ in both size,[31] shape,[45] and sustained loads,[26] it is possible that matrix distribution within each insertion

site has been optimized with age. Recent work has revealed lateral variations in collagen organization across the tibial insertion,[46] and proteoglycan content may also change laterally across the immature femoral insertion.[10] Here, FTIRI analysis of the mature insertions found no significant lateral variations in GAG (data not shown). Future work will incorporate other analysis techniques to quantitatively characterize composition and structure across the full three-dimensional volume of the ACL-to-bone insertion and correlate these properties to mechanical function.

Limitations of this study include the use of a quadrupedal animal model and the exclusive study of female specimens. Although the bovine knee differs from the human knee in terms of anatomy and loading, the bovine ACL is better match for the human ACL in terms of size and proportion compared to most other commonly used animal models.[25,47] Additionally, the ACL is a primary force contributor in both quadruped and human knee movement.[48] Thus, despite apparent differences in knee kinematics, it is expected that the substantial post-natal remodeling observed in the bovine model can also be extrapolated to humans. Since species-related differences in matrix content can exist between quadrupedal versus bipedal joints, analyses in this study have focused on spatial differences in matrix content, rather than on the magnitudes of the matrix parameters. The restriction of this study to female specimens serves to reduce inter-sample variation, given the well-established gender-related differences in knee anatomy and biomechanics.[49] Additionally, as the higher prevalence of ACL injury among women may be related to sex-specific hormones,[50] the study of the ACL in female animal models is particularly important for elucidating these sex-specific differences. Future work will focus on validating study findings in human tissues and extending the characterization to both male and female joints.

In this study, both region- and age-dependent changes in matrix composition and organization were found at the mature ACL-to-bone insertion, which reflect adaptations to the complex loads sustained at the ligament-to-bone enthesis. Collectively, these findings may be used to guide current efforts to develop biomimetic grafts for interface tissue engineering and integrative soft tissue regeneration. In terms of tissue engineering scaffold design, the exponential increase in mineral content across the ACL-to-bone insertion can be approximated as a step-wise increase in mineral content and can be recapitulated by a stratified design consisting of contiguous mineral-free and mineral-containing regions. Maintaining relative mineral to collagen content also appears to be a salient feature in recapitulating the composition and structure of the insertion. Furthermore, the age-related changes in tissue composition and organization underscore the importance of physiologic loading in enthesis maturation and indicate that mechanical stimulation may also be harnessed to guide tissue regeneration. The results from this study enhance current understanding of the structure-function relationships at soft tissue-to-bone interfaces and provide guidance for integrative soft tissue repair strategies. Moreover, these findings can be extended to other critical attachments, such as the supraspinatus tendon-to-bone insertion in the rotator cuff. It is expected that these transitions, found throughout key load-bearing joints, will similarly undergo significant postnatal remodeling.

AUTHORS' CONTRIBUTIONS

DQ, SDS, and HHL: Study design. DQ and SDS: Study conduct. DQ: Data collection. DQ: Data analysis. DQ, ALB, NP, SBD, and HHL: Data interpretation. DQ, SDS, ALB, NP, SBD, and HHL: Manuscript preparation and editing.

ACKNOWLEDGMENTS

The authors thank Mr. Anthony Labissiere and Ms. Lyudmila Spevak of the Hospital for Special Surgery for assistance with histology and data acquisition, respectively. This study was supported by the Presidential Early Career Award for Scientists and Engineers (HHL), NIH-NIAMS (AR055280, HHL), a NIH Core Center Grant (AR046121, ALB), the NIH Ruth L. Kirschstein National Research Service Award T32 (AR059038, DQ), and the National Science Foundation Graduate Research Fellowship (SDS).

REFERENCES

1. Cooper RR, Misol S. 1970. Tendon and ligament insertion. A light and electron microscopic study. J Bone Joint Surg Am 52:1–20.
2. Benjamin M, Evans EJ, Copp L. 1986. The histology of tendon attachments to bone in man. J Anat 149:89–100.
3. Benjamin M, Ralphs JR. 1998. Fibrocartilage in tendons and ligaments—an adaptation to compressive load. J Anat 193: 481–494.
4. Petersen W, Tillmann B. 1999. Structure and vascularization of the cruciate ligaments of the human knee joint. Anat Embryol (Berl) 200:325–334.
5. Niyibizi C, Sagarrigo VC, Gibson G, et al. 1996. Identification and immunolocalization of type X collagen at the ligament-bone interface. Biochem Biophys Res Commun 222: 584–589.
6. Wang IE, Mitroo S, Chen FH, et al. 2006. Age-dependent changes in matrix composition and organization at the ligament-to-bone insertion. J Orthop Res 24:1745–1755.
7. Moffat KL, Sun WH, Pena PE, et al. 2008. Characterization of the structure-function relationship at the ligament-to-bone interface. Proc Natl Acad Sci USA 105:7947–7952.
8. Wopenka B, Kent A, Pasteris JD, et al. 2008. The tendon-to-bone transition of the rotator cuff: a preliminary Raman spectroscopic study documenting the gradual mineralization across the insertion in rat tissue samples. Appl Spectrosc 62:1285–1294.
9. Schwartz AG, Pasteris JD, Genin GM, et al. 2012. Mineral distributions at the developing tendon-to-bone enthesis. PLoS ONE 7:e48630.
10. Spalazzi JP, Boskey AL, Pleshko N, et al. 2013. Quantitative mapping of matrix content and distribution across the ligament-to-bone insertion. PLoS ONE 8:e74349.

11. Woo SL, Wu C, Dede O, et al. 2006. Biomechanics and anterior cruciate ligament reconstruction. J Orthop Surg 1:2.
12. Friedman MJ, Sherman OH, Fox JM, et al. 1985. Autogeneic anterior cruciate ligament (ACL) anterior reconstruction of the knee. A review. Clin Orthop 196:9–14.
13. Getelman MH, Friedman MJ. 1999. Revision anterior cruciate ligament reconstruction surgery. J Am Acad Orthop Surg 7:189–198.
14. Lu HH, Thomopoulos S. 2013. Functional attachment of soft tissues to bone: development, healing, and tissue engineering. Annu Rev Biomed Eng 15:201–226.
15. Gao J, Messner K. 1996. Quantitative comparison of soft tissue-bone interface at chondral ligament insertions in the rabbit knee joint. J Anat 188:367–373.
16. Khanarian NT, Boushell MK, Spalazzi JP, et al. 2014. FTIR-I compositional mapping of the cartilage-to-bone interface as a function of tissue region and age. J Bone Miner Res 29: 2643–2652.
17. Kim M, Bi X, Horton WE, et al. 2005. Fourier transform infrared imaging spectroscopic analysis of tissue engineered cartilage: histologic and biochemical correlations. J Biomed Opt 10:031105.
18. Bi X, Yang X, Bostrom MP, et al. 2006. Fourier transform infrared imaging spectroscopy investigations in the pathogenesis and repair of cartilage. Biochim Biophys Acta 1758: 934–941.
19. Gadaleta SJ, Landis WJ, Boskey AL, et al. 1996. Polarized FT-IR microscopy of calcified turkey leg tendon. Connect Tissue Res 34:203–211.
20. Bi X, Li G, Doty SB, et al. 2005. A novel method for determination of collagen orientation in cartilage by Fourier transform infrared imaging spectroscopy (FT-IRIS). Osteoarthritis Cartilage 13:1050–1058.
21. Benjamin M, Tyers RN, Ralphs JR. 1991. Age-related changes in tendon fibrocartilage. J Anat 179:127–136.
22. Murray MM, Magarian EM, Harrison SL, et al. 2010. The effect of skeletal maturity on functional healing of the anterior cruciate ligament. J Bone Joint Surg Am 92: 2039–2049.
23. Woo SL, Hollis JM, Adams DJ, et al. 1991. Tensile properties of the human femur-anterior cruciate ligament-tibia complex. The effects of specimen age and orientation. Am J Sports Med 19:217–225.
24. Legnani C, Terzaghi C, Borgo E, et al. 2011. Management of anterior cruciate ligament rupture in patients aged 40 years and older. J Orthop Traumatol 12:177–184.
25. Proffen BL, McElfresh M, Fleming BC, et al. 2012. A comparative anatomical study of the human knee and six animal species. Knee 19:493–499.
26. Spalazzi JP, Gallina J, Fung-Kee-Fung SD, et al. 2006. Elastographic imaging of strain distribution in the anterior cruciate ligament and at the ligament-bone insertions. J Orthop Res 24:2001–2010.
27. Strocchi R, De Pasquale V, Facchini A, et al. 1996. Age-related changes in human anterior cruciate ligament (ACL) collagen fibrils. Ital J Anat Embryol 101:213–220.
28. Shadwick RE. 1990. Elastic energy storage in tendons: mechanical differences related to function and age. J Appl Physiol 68:1033–1040.
29. Tuite DJ, Renstrom PA, O'Brien M. 1997. The aging tendon. Scand J Med Sci Sports 7:72–77.
30. Esquisatto MA, Joazeiro PP, Pimentel ER, et al. 2007. The effect of age on the structure and composition of rat tendon fibrocartilage. Cell Biol Int 31:570–577.
31. Harner CD, Baek GH, Vogrin TM, et al. 1999. Quantitative analysis of human cruciate ligament insertions. Arthroscopy 15:741–749.
32. Hunziker EB, Ludi A, Herrmann W. 1992. Preservation of cartilage matrix proteoglycans using cationic dyes chemically related to ruthenium hexaammine trichloride. J Histochem Cytochem 40:909–917.
33. Camacho NP, West P, Torzilli PA, et al. 2001. FTIR microscopic imaging of collagen and proteoglycan in bovine cartilage. Biopolymers 62:1–8.
34. Boskey AL, Pleshko N, Doty SB, et al. 1992. Applications of FTIR microscopy to the study of mineralization in bone and cartilage. Cells Mater 2:209–220.
35. Rieppo L, Saarakkala S, Narhi T, et al. 2010. Quantitative analysis of spatial proteoglycan content in articular cartilage with Fourier transform infrared imaging spectroscopy: critical evaluation of analysis methods and specificity of the parameters. Microsc Res Tech 73:503–512.
36. Paschalis EP, DiCarlo E, Betts F, et al. 1996. FTIR microspectroscopic analysis of human osteonal bone. Calcif Tissue Int 59:480–487.
37. Thomopoulos S, Marquez JP, Weinberger B, et al. 2006. Collagen fiber orientation at the tendon to bone insertion and its influence on stress concentrations. J Biomech 39: 1842–1851.
38. Genin GM, Kent A, Birman V, et al. 2009. Functional grading of mineral and collagen in the attachment of tendon to bone. Biophys J 97:976–985.
39. Gao J, Messner K, Ralphs JR, et al. 1996. An immunohistochemical study of enthesis development in the medial collateral ligament of the rat knee joint. Anat Embryol (Berl) 194:399–406.
40. Matyas JR, Anton MG, Shrive NG, et al. 1995. Stress governs tissue phenotype at the femoral insertion of the rabbit MCL. J Biomech 28:147–157.
41. Messner K. 1997. Postnatal development of the cruciate ligament insertions in the rat knee. morphological evaluation and immunohistochemical study of collagens types I and II. Acta Anat 160:261–268.
42. Niyibizi C, Visconti CS, Kavalkovich K, et al. 1995. Collagens in an adult bovine medial collateral ligament: immunofluorescence localization by confocal microscopy reveals that type XIV collagen predominates at the ligament-bone junction. Matrix Biol 14:743–751.
43. Hems T, Tillmann B. 2000. Tendon entheses of the human masticatory muscles. Anat Embryol 202:201–208.
44. Thomopoulos S, Kim HM, Rothermich SY, et al. 2007. Decreased muscle loading delays maturation of the tendon enthesis during postnatal development. J Orthop Res 25: 1154–1163.
45. Ziegler CG, Pietrini SD, Westerhaus BD, et al. 2011. Arthroscopically pertinent landmarks for tunnel positioning in single-bundle and double-bundle anterior cruciate ligament reconstructions. Am J Sports Med 39:743–752.
46. Zhao L, Thambyah A, Broom ND. 2014. A multi-scale structural study of the porcine anterior cruciate ligament tibial enthesis. J Anat 224:624–633.
47. Xerogeanes JW, Fox RJ, Takeda Y, et al. 1998. A functional comparison of animal anterior cruciate ligament models to the human anterior cruciate ligament. Ann Biomed Eng 26: 345–352.
48. Nesbitt RJ, Herfat ST, Boguszewski DV, et al. 2014. Primary and secondary restraints of human and ovine knees for simulated in vivo gait kinematics. J Biomech 47:2022–2027.
49. Chandrashekar N, Mansouri H, Slauterbeck J, et al. 2006. Sex-based differences in the tensile properties of the human anterior cruciate ligament. J Biomech 39: 2943–2950.
50. Wojtys EM, Huston LJ, Lindenfeld TN, et al. 1998. Association between the menstrual cycle and anterior cruciate ligament injuries in female athletes. Am J Sports Med 26: 614–619.